

Fuzzy-Based Antiswing Control for Variable-Length Cable-Suspended Aerial Transportation Systems Considering the Hook Effect

Hai Yu^{ID}, Student Member, IEEE, Yi Chai^{ID}, Zhichao Yang, Jianda Han^{ID}, Member, IEEE,
Yongchun Fang^{ID}, Senior Member, IEEE, and Xiao Liang^{ID}, Senior Member, IEEE

Abstract—As a low-cost cargo delivery manner, cable-suspended aerial transportation system is highly regarded by researchers. However, existing works seldom consider the relative distance adjustment between the payload and the multirotor, which greatly limits the application scope, such as tunnel traversing or payload releasing. In addition, treating the hook and the payload as a single point mass while ignoring the hook effect results in an inaccurate description of the dynamic model. To address the aforementioned problems, the dynamic model of the variable-length cable-suspended aerial transportation system is established accurately through Lagrange's equation with consideration of the motion of the multirotor, the payload, and the hook. Subsequently, an adaptive control method is presented through energy-based analysis, and swing angle related fuzzy rules are established to dynamically adjust the control parameters, which can simultaneously achieve multirotor positioning, payload hoisting/lowering, and hook/payload swing suppression. Moreover, the cable length is constrained within a feasible range by an elaborately designed auxiliary control signal. Lyapunov techniques and LaSalle's invariance theorem are utilized to prove the asymptotic convergence of the closed-loop system. Finally, a series of simulations are conducted to verify the control performance of the designed method.

Index Terms—Aerial transportation systems, fuzzy-based antiswing, hook effect, payload hoisting/lowering.

I. INTRODUCTION

NOWADAYS, with the rapid development of electronics and informatics, the applications of robots have greatly saved labor costs, while keeping people away from jobs with harsh environments and high risks. Particularly, thanks to the vertical take-off and landing ability, strong mobility and flexibility, multirotor autonomous aerial vehicles have been widely utilized

Received 15 August 2024; revised 12 October 2024; accepted 24 October 2024. Date of publication 29 October 2024; date of current version 5 February 2025. This work was supported in part by the National Natural Science Foundation of China under Grant 623B2054, Grant 62273187, and Grant 62233011, in part by the Natural Science Foundation of Tianjin under Grant 23JCQNJC01930, and in part by the Postdoctoral Fellowship Program of CPSF under Grant GZC20231173. Recommended by Associate Editor C. Yang. (Corresponding author: Xiao Liang.)

Hai Yu, Yi Chai, Zhichao Yang, Jianda Han, Yongchun Fang, and Xiao Liang are with the Institute of Robotics and Automatic Information System, College of Artificial Intelligence, and Tianjin Key Laboratory of Intelligent Robotics, Nankai University, Tianjin 300350, China, and also with the Institute of Intelligence Technology and Robotic Systems, Shenzhen Research Institute, Nankai University, Shenzhen 518083, China (e-mail: yuhai@mail.nankai.edu.cn; chaiyi@nankai.edu.cn; yangzc@mail.nankai.edu.cn; hanjianda@nankai.edu.cn; fangyc@nankai.edu.cn; liangx@nankai.edu.cn).

Digital Object Identifier 10.1109/TFUZZ.2024.3487579

in search and rescue, fire fighting, environmental monitoring, etc [1], [2], [3], [4], [5], [6]. Since they are not affected by the terrain constraints, the application for cargo transportation is very convenient and of great significance, especially in postdisaster relief and materials delivery.

In the last few years, as one of the important aerial cargo delivery systems, the cable-suspended aerial transportation system has attracted the attention of many researchers. Plenty of control and planning schemes [7], [8], [9], [10], [11], [12], [13] have been designed and applied to the cable-suspended aerial transportation system. Sreanath et al. [7] proposed a nonlinear geometric control law based on the established coordinate-free dynamics model, which has the ability to track multirotor attitude and payload position. To deal with unknown wind disturbances, an uncertainty and disturbance estimator-based path-following controller [8] is developed to asymptotically stabilize the cable-suspended aerial transportation system. Also, to handle the presence of unknown air turbulence, a robust control scheme [9] is designed based on the robust integral of the sign of the error. In [10], the cable-suspended aerial transportation system is established as a differentially flat hybrid system. Then, employing the complementarity constraints and reformulating the obstacle avoidance from nonconvex constraints into smooth ones, a planning method is designed to generate agile multirotor motions. By integrating a fault-tolerant control with a fuzzy logic system, an adaptive fuzzy control law [11] is developed for the helicopter cable-suspended payload transportation system to address the actuator fault, system uncertainty, and disturbances. To pass through windows and avoid obstacles, an aggressive payload position and swing angle trajectory generation approach [12] is designed by imposing payload acceleration limitations. A minimum-time trajectory planning method is provided in [13], which ensures the continuity of the desired trajectory acceleration and avoids undesired motor vibrations by utilizing jerk signals as inputs.

Nevertheless, it is difficult for the aerial transportation system with fixed-length cable to accomplish such tasks as going through a tunnel or releasing the payload. On the one hand, when crossing through the tunnel, the multirotor or the payload may hit the obstacle, e.g., ground and walls. Therefore, shortening the relative distance between the multirotor and the payload before traversing makes the flight process feasible. On the other hand, when executing the payload landing mission, it is necessary to

reduce the altitude of the multirotor to achieve payload landing. However, due to the ground effect, the airflow will cause payload swing and multirotor shake violently, thus, the multirotor must keep a long enough safe distance from the ground surface. In addition, a flexible relative distance between the multirotor and the payload can achieve dynamic obstacle avoidance so as to ensure the smooth transportation of the payload. Facing these demands, the aerial transportation system with variable-length cable is studied in some recent research [14], [15], [16], [17], [18], [19], [20]. Geometric nonlinear control methods are designed in [14] and [15], which aim at realizing the tracking objective of multirotor attitude, cable length, and payload position. Payload antiswing methods are introduced in [16] and [17] for smooth payload transportation. In [18], an adaptive trajectory tracking control scheme is developed to enable payload landing onto the mobile platform, and Yu et al. [19] further enhanced the system's behavioral autonomy by mounting an onboard camera on the multirotor. In addition, Li et al. [20] proposed an optimization-based trajectory planning algorithm to cross narrow gap.

However, considering the practical transportation systems, the cargo is always suspended on a hook at the end of the cable. While most current studies are based on the assumption that the suspended hook and payload are regarded as a single point of mass, which implies that the motion of the hook is ignored. In fact, the center of gravity (CoG) of the hook is at some distance from the CoG of the payload. Therefore, the multirotor's motion will lead to sway of both the payload and the hook, and the motion of the hook will also affect the payload, which means the cable-suspended aerial transportation system has a double-pendulum swing effect. Since there is no control input directly acting on the payload or hook swing, the introduction of the double-pendulum increases the degrees of freedom of the underactuated part. To overcome the challenges posed by the double-pendulum effect in payload transportation, several studies have been conducted to achieve hook/payload swing elimination in recent studies [21], [22], [23], [24]. By employing the simplified planar model, a framework combining model predictive control with PD control [21], as well as an online trajectory planning method [22], is developed separately to achieve hook/payload sway suppression. In addition, by incorporating payload and hook swing angles information, Liang et al. [23] designed an antiswing controller for the three-dimensional system model. Then, the enhanced coupling signals are introduced in [24] to further improve the swing suppression performance. However, these works are all focused on the aerial transportation system with fixed-length cable and do not consider variable-length cable scenarios. As a result, the motion of the multirotor, the cable, the hook, and the payload exhibits strong nonlinearity and complex dynamic coupling, making the precise control significantly complicated.

To tackle these problems, a nonlinear adaptive control method is proposed for the aerial transportation systems with variable-length cable considering the hook effect, which can effectively complete payload delivery task. The main contributions can be summarized as follows.

- 1) Although some studies have been implemented on the variable-length cable-suspended aerial transportation system [14], [15], [16], [17], [18], [19], [20], the payload and its hook are considered as one unit in the existing works, which cannot reflect the dynamics of the actual transportation system. However, high-performance control usually need precise dynamic model, especially for such underactuated systems. To this end, an accurate dynamic model is established for the variable-length cable-suspended aerial transportation system with the consideration of the hook effect.
- 2) Inspired by the barrier Lyapunov function, an auxiliary term is introduced to the control structure to ensure that the cable length is always within a positive set range, which is the important condition to avoid collision between the multirotor and the hook. In addition to guaranteeing the safety of the system, it is also a necessary condition for the subsequent stability analysis.
- 3) Without any model linearization or simplification operations, a nonlinear adaptive controller is proposed based on the system energy analysis. By constructing fuzzy rules regarding the hook and payload swing angles, the control gains are modified online to enhance the hook/payload swing suppression ability. Moreover, with the help of Lyapunov techniques and LaSalle's invariance theorem, the closed-loop system is guaranteed to be asymptotic stable.

The rest of this article is organized as follows. Considering the hook effect, the dynamic model of the aerial transportation system with variable-length cable is established in Section II, where the control problem is also stated. The control law design, as well as the stability analysis, is provided in Section III. In Section IV, several groups of simulations are provided to show the performance of the control system. Finally, Section V concludes this article.

Notation: For a vector $\mathbf{h} = [h_1, \dots, h_n]^\top \in \mathbb{R}^n$, define $\text{sgn}(\mathbf{h}) = [\text{sgn}(h_1), \dots, \text{sgn}(h_n)]^\top$, and $\text{diag}(\mathbf{h})$ is a diagonal matrix with diagonal elements of h_1, \dots, h_n . To facilitate the descriptions, let $C_{1x}, C_{1y}, S_{1x}, S_{1y}, C_{2x}, C_{2y}, S_{2x}, S_{2y}, C_{1x-2x}, S_{1x-2x}$ denote the abbreviations of $\cos \theta_{1x}, \cos \theta_{1y}, \sin \theta_{1x}, \sin \theta_{1y}, \cos \theta_{2x}, \cos \theta_{2y}, \sin \theta_{2x}, \sin \theta_{2y}, \cos(\theta_{1x} - \theta_{2x}), \sin(\theta_{1x} - \theta_{2x})$.

II. DYNAMIC MODELING AND PROBLEM STATEMENTS

The schematic configuration of the aerial transportation system with variable-length cable is shown in Fig. 1. A cable length adjustment mechanism is mounted at the bottom of the multirotor, which is utilized to hoist/lower the payload. A hook is attached to the end of the cable, and the payload is suspended from the hook. $M, m_h, m_p \in \mathbb{R}$ denotes the multirotor, hook, and payload masses, $g \in \mathbb{R}$ is the gravitational acceleration, $l \in \mathbb{R}$ denotes the cable length. The distance between the hook and the payload is denoted by $c \in \mathbb{R}$. $\xi = [x, y, z]^\top \in \mathbb{R}^3$ denotes the multirotor position. $\xi_h = [x_h, y_h, z_h]^\top \in \mathbb{R}^3$ and

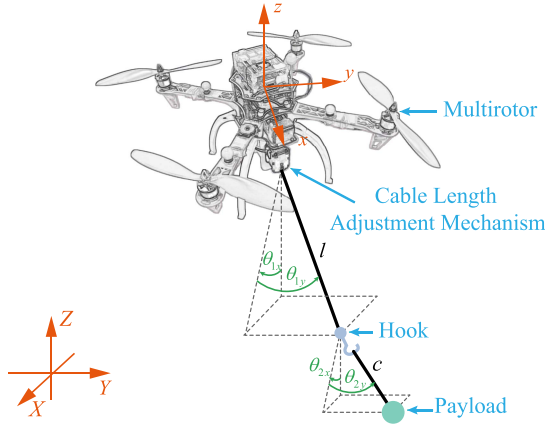


Fig. 1. Aerial transportation system with variable-length cable considering the hook effect.

$\xi_p = [x_p, y_p, z_p]^\top \in \mathbb{R}^3$ denote the hook and the payload position, respectively. $\Theta_1(t) = [\theta_{1x}(t), \theta_{1y}(t)]^\top \in \mathbb{R}^2$, $\Theta_2(t) = [\theta_{2x}(t), \theta_{2y}(t)]^\top \in \mathbb{R}^2$ are the hook's and payload's swing signals.

Considering the actual transportation systems, as well as the recent research works [25], [26], [27], [28], [29], the following reasonable assumptions are given.

Assumption 1: The suspension cables between the multirotor and the hook, as well as between the hook and the payload, are inelastic and massless.

Assumption 2: The hook and the payload are always under the multirotor, implying that the swing angles $\theta_{1x}, \theta_{1y}, \theta_{2x}$, and θ_{2y} are within the range of $(-\pi/2, \pi/2)$.

The relation among the hook position ξ_h , the payload position ξ_p , and the multirotor position ξ can be provided as

$$\xi_h = [x + lS_{1x}C_{1y}, y + lS_{1y}, z - lC_{1x}C_{1y}]^\top \quad (1)$$

$$\begin{aligned} \xi_p = & [x + lS_{1x}C_{1y} + cS_{2x}C_{2y}, y + lS_{1y} + cS_{2y}, \\ & z - lC_{1x}C_{1y} - cC_{2x}C_{2y}]^\top. \end{aligned} \quad (2)$$

It should be noted that this article focuses on the translation motion of the multirotor, and the motion of the hook and the payload. To establish the system model, the generalized coordinate of the system is selected as $\mathbf{q} = [x, y, z, l, \theta_{1x}, \theta_{1y}, \theta_{2x}, \theta_{2y}]^\top \in \mathbb{R}^8$. Subsequently, define $L = T - P$ as the Lagrangian, $T = \frac{1}{2}M\dot{\xi}^\top\dot{\xi} + \frac{1}{2}m_h\dot{\xi}_h^\top\dot{\xi}_h + \frac{1}{2}m_p\dot{\xi}_p^\top\dot{\xi}_p$ and $P = Mgz + m_hgz_h + m_pgz_p$ are the kinematic and potential energy, $\mathbf{Q} = \delta W/\delta \mathbf{q} \in \mathbb{R}^8$ represents the generalized force, $\delta \mathbf{q}$ is the virtual displacement, and δW is the virtual work. Let $f_x, f_y, f_z \in \mathbb{R}$ denote the three elements of the multirotor applied thrust force, $f_l \in \mathbb{R}$ denote the actuating force generated by the cable length adjustment mechanism. The virtual work can be described as $\delta W = [f_x, f_y, f_z]^\top \delta \xi + f_l \delta l + \mathbf{f}_{c\xi}^\top \delta \xi + \mathbf{f}_{cl} \delta l + \mathbf{f}_{ch} \delta \xi_h + \mathbf{f}_{cp} \delta \xi_p$, where $\mathbf{f}_{c\xi} = -D\xi$, $\mathbf{f}_{cl} = -d_l \dot{l}$, $\mathbf{f}_{ch} = -d_h \dot{\xi}_h$ and $\mathbf{f}_{cp} = -d_p \dot{\xi}_p$ are resistances acting on the multirotor, cable, hook, and payload. $D\xi = \text{diag}([d_x, d_y, d_z]) \in \mathbb{R}_+^{3 \times 3}$ and $d_l, d_h, d_p \in \mathbb{R}_+$ are the resistance coefficients. Thus, with the

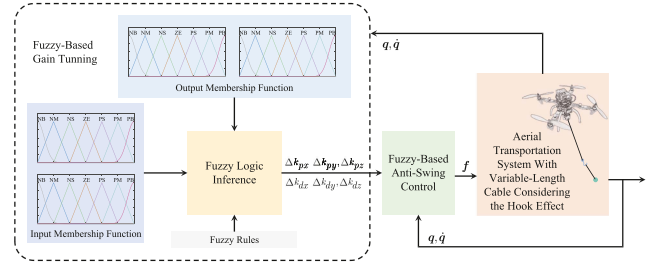


Fig. 2. Block diagram of the designed control algorithm.

help of the Lagrange's equation: $\frac{d}{dt} \frac{\partial L}{\partial \dot{q}} - \frac{\partial L}{\partial q} = \mathbf{Q}$, the dynamic model of the system can be established as

$$M_c(\mathbf{q})\ddot{\mathbf{q}} + V_c(\mathbf{q}, \dot{\mathbf{q}})\dot{\mathbf{q}} + \mathbf{G}(\mathbf{q}) = \mathbf{u} + \mathbf{F}_r \quad (3)$$

where $\mathbf{u} = [\mathbf{f}^\top, 0, 0, 0, 0]^\top = [f_x, f_y, f_z, f_l, 0, 0, 0, 0]^\top \in \mathbb{R}^8$ is the control input vector, $M_c(\mathbf{q}) \in \mathbb{R}^{8 \times 8}$ is the inertia matrix, $V_c(\mathbf{q}, \dot{\mathbf{q}}) \in \mathbb{R}^{8 \times 8}$ is the centripetal-coriolis matrix, $\mathbf{G}(\mathbf{q}) \in \mathbb{R}^8$ is the gravity vector, $\mathbf{F}_r = [f_{rx}, f_{ry}, f_{rz}, f_{rl}, f_{r\theta_{1x}}, f_{r\theta_{1y}}, f_{r\theta_{2x}}, f_{r\theta_{2y}}]^\top$ is the resistance forces vector. The detailed form of (3) is given in Appendix A. Regarding the underactuated system (3), one can obtain the following important properties without much difficulty.

Property 1: Matrix $M_c(\mathbf{q})$ is positive definite.

Property 2: Matrices $V_c(\mathbf{q}, \dot{\mathbf{q}})$ and $M_c(\mathbf{q})$ satisfy the skew-symmetric relationship: $\boldsymbol{\eta}^\top (\frac{1}{2}M_c - V_c)\boldsymbol{\eta} = 0, \forall \boldsymbol{\eta} \in \mathbb{R}^8$.

To realize smooth payload transportation, the objective of this article can be concluded as follows.

- 1) Design a feedback control law that drives the multirotor to the desired position $\xi_d = [x_d, y_d, z_d]^\top$ and adjusts the variable-length cable to the desired length l_d , while eliminating the hook and the payload swing rapidly, which can be quantified as

$$\xi \rightarrow \xi_d, l \rightarrow l_d, \Theta_1 \rightarrow [0, 0]^\top, \Theta_2 \rightarrow [0, 0]^\top. \quad (4)$$

- 2) Restrict the cable length within the range of (l_{\min}, l_{\max}) , where l_{\min} and $l_{\max} \in \mathbb{R}^+$ are the lower and upper bounds of the cable length, respectively.

Fig. 2 presents the block diagram of the proposed method.

III. CONTROLLER DESIGN AND STABILITY ANALYSIS

This section will detail both the adaptive control scheme design and the corresponding stability analysis.

A. Controller Design

To facilitate the subsequent controller development and analysis, define a composite vector $\alpha = [x, y, z, l]^\top \in \mathbb{R}^4$ consisting of the multirotor position and the variable-length cable, whose desired value is $\alpha_d = [x_d, y_d, z_d, l_d]^\top$. Then, the error vector of the composite signal is defined as $e_\alpha = \alpha(t) - \alpha_d = [e_x(t), e_y(t), e_z(t), e_l(t)]^\top \in \mathbb{R}^4$, and its time derivative is $\dot{e}_\alpha = \dot{\alpha}$. Thus, the generalized state error $e_q \in \mathbb{R}^8$ takes the following form:

$$e_q = \mathbf{q} - \mathbf{q}_d = [\mathbf{e}_\alpha^\top, \Theta_1^\top, \Theta_2^\top]^\top. \quad (5)$$

For the sake of controller design, the energy storage function of the system is first presented as

$$\begin{aligned} E = & \frac{1}{2} \dot{\mathbf{q}}^\top M_c \dot{\mathbf{q}} + (m_h + m_p) gl (1 - C_{1x} C_{1y}) \\ & + m_p g c (1 - C_{2x} C_{2y}). \end{aligned} \quad (6)$$

Subsequently, according to the dynamic model (3), invoking Property 2 and taking the time derivative of (6) leads to

$$\begin{aligned} \dot{E} = & \dot{\mathbf{q}}^\top \left(M_c \ddot{\mathbf{q}} + \frac{1}{2} \dot{M}_c \dot{\mathbf{q}} \right) + (m_h + m_p) g \dot{l} (1 - C_{1x} C_{1y}) \\ & + (m_h + m_p) g l \left(\dot{\theta}_{1x} S_{1x} C_{1y} + \dot{\theta}_{1y} C_{1x} S_{1y} \right) \\ & + m_p g c \left(\dot{\theta}_{2x} S_{2x} C_{2y} + \dot{\theta}_{2y} C_{2x} S_{2y} \right) \\ = & \dot{\mathbf{q}}^\top \left(\frac{1}{2} \dot{M}_c - V_c \right) \dot{\mathbf{q}} - \dot{\mathbf{q}}^\top \mathbf{G} + \dot{\alpha} \mathbf{f} + \dot{\mathbf{q}}^\top \mathbf{F}_r \\ & + (m_h + m_p) g \dot{l} (1 - C_{1x} C_{1y}) \\ & + (m_h + m_p) g l \left(\dot{\theta}_{1x} S_{1x} C_{1y} + \dot{\theta}_{1y} C_{1x} S_{1y} \right) \\ & + m_p g c \left(\dot{\theta}_{2x} S_{2x} C_{2y} + \dot{\theta}_{2y} C_{2x} S_{2y} \right) \\ = & \dot{\alpha} [\mathbf{f} - (M + m_h + m_p) g \mathbf{r}_3 + (m_h + m_p) g \mathbf{r}_4] + \dot{\mathbf{q}}^\top \mathbf{F}_r \\ = & \dot{\mathbf{e}}_\alpha^\top [\mathbf{f} - (M + m_h + m_p) g \mathbf{r}_3 + (m_h + m_p) g \mathbf{r}_4] + \dot{\mathbf{q}}^\top \mathbf{F}_r \\ = & \dot{\mathbf{e}}_\alpha^\top [\mathbf{f} - (M + m_h + m_p) g \mathbf{r}_3 + (m_h + m_p) g \mathbf{r}_4 - \Phi_\alpha] \\ & - [\dot{\Theta}_1^\top, \dot{\Theta}_2^\top] \Psi [\dot{\Theta}_1^\top, \dot{\Theta}_2^\top]^\top \end{aligned} \quad (7)$$

wherein $\mathbf{r}_3 = [0, 0, 1, 0]^\top$ and $\mathbf{r}_4 = [0, 0, 0, 1]^\top$ are two unit vectors. Φ_α takes the form of $\Phi_\alpha = [\phi_x^\top \omega_x, \phi_y^\top \omega_y, \phi_z^\top \omega_z, \phi_l^\top \omega_l]^\top$, where the composite velocity signal vectors $\phi_x, \phi_y, \phi_z, \phi_l \in \mathbb{R}^3$ as well as the damping coefficient vectors $\omega_x, \omega_y, \omega_z, \omega_l \in \mathbb{R}^3$ are represented in Appendix B. $\Psi \in \mathbb{R}^{4 \times 4}$ is a positive definite matrix given in Appendix C.

To ensure that E is nonnegative, the length of the cable need to be always positive, i.e., $l > 0$, which is always true for the fixed-length aerial transportation system. However, in this article, in the presence of payload hoisting/lowering control, the positive cable length is not easy to be guaranteed theoretically due to various factors such as overshoots. Besides, there should be some distance between the multirotor and the hook to ensure the safety during flight. Hence, an auxiliary term is designed to limit the cable length within a given range (l_{\min}, l_{\max}). Define $\varpi_\pi = \frac{2\pi}{(l_{\max} - l_{\min})^2}$, $\varpi_l = \frac{l_{\min} + l_{\max}}{2}$. The auxiliary term is designed as

$$\begin{aligned} f_{l\rho} = k_s & \frac{\sin(\varpi_\pi(l - \varpi_l)^2) \varpi_\pi(l - \varpi_l) \rho^2}{\cos^2(\varpi_\pi(l - \varpi_l)^2)} \\ & + k_s \sec(\varpi_\pi(l - \varpi_l)^2) \end{aligned} \quad (8)$$

where k_s is a positive control gain. ρ is the auxiliary signal of e_l defined as

$$\begin{aligned} \rho = e_l + \int_0^t \varrho(\tau) d\tau, \varrho = -\eta \rho \\ \Rightarrow \dot{\rho} = \dot{e}_l - \eta \rho, \varrho(0) = -\eta \rho(0), \rho(0) = e_l(0) \end{aligned} \quad (9)$$

where η is a positive control parameter.

Subsequently, under the form of E , the control scheme can be elaborately designed as follows:

$$\begin{aligned} \mathbf{f} = & -K_p \mathbf{e}_\alpha - K_d \dot{\mathbf{e}}_\alpha - f_{l\rho} \mathbf{r}_4 + \hat{\Phi}_\alpha \\ & + (M + m_h + m_p) g \mathbf{r}_3 - (m_h + m_p) g \mathbf{r}_4 \end{aligned} \quad (10)$$

where $K_p, K_d \in \mathbb{R}_+^{4 \times 4}$ represent positive definite diagonal gain matrices. $\hat{\Phi}_\alpha = [\phi_x^\top \dot{\omega}_x, \phi_y^\top \dot{\omega}_y, \phi_z^\top \dot{\omega}_z, \phi_l^\top \dot{\omega}_l]^\top$ is the to-be-designed online estimation of Φ_α . The online update rates for the damping coefficient vectors are designed as

$$\begin{aligned} \dot{\omega}_x = & -\Upsilon_x \phi_x \dot{e}_x, \dot{\omega}_y = -\Upsilon_y \phi_y \dot{e}_y \\ \dot{\omega}_z = & -\Upsilon_z \phi_z \dot{e}_z, \dot{\omega}_l = -\Upsilon_l \phi_l \dot{e}_l \end{aligned} \quad (11)$$

where $\Upsilon_x, \Upsilon_y, \Upsilon_z, \Upsilon_l \in \mathbb{R}_+^{3 \times 3}$ are positive definite diagonal matrices.

Due to the underactuated characteristic of the system, there is no control input directly acting on the payload and the hook. The swing of the payload and hook can only be suppressed indirectly through the motion of the multirotor. Thus, by considering the information of swing angles, fuzzy rules are established to dynamically adjust the control gains of the multirotor to improve the payload and hook swing elimination performance. Unlike conventional fuzzy methods, the position and velocity errors of the multirotor are not directly utilized as inputs for the fuzzy rules. Instead, signals related to the hook and payload swing angles are used, which are empirically selected as

$$\begin{aligned} \mathbf{E} = [E_x, E_y, E_z]^\top = & \text{diag}(\text{sgn}(e_\xi)) [l S_{1x} C_{1y} + c S_{2x} C_{2y} \\ & l S_{1y} + c S_{2y}, ld - l C_{1x} C_{1y} + c(1 - C_{2x} C_{2y})]^\top \end{aligned} \quad (12)$$

$$\begin{aligned} \mathbf{EC} = [EC_x, EC_y, EC_z]^\top = & -\text{diag}(\text{sgn}(\dot{e}_\xi)) [l S_{1x} C_{1y} \\ & + l \dot{\theta}_{1x} C_{1x} C_{1y} - l \dot{\theta}_{1y} S_{1x} S_{1y} + c \dot{\theta}_{2x} C_{2x} C_{2y} \\ & - c \dot{\theta}_{2y} S_{2x} S_{2y}, l S_{1y} + l \dot{\theta}_{1y} C_{1x} + c \dot{\theta}_{2y} C_{2x} \\ & - l C_{1x} C_{1y} + l \dot{\theta}_{1x} S_{1x} C_{1y} + l \dot{\theta}_{1y} C_{1x} S_{1y} \\ & + c \dot{\theta}_{2x} S_{2x} C_{2y} + c \dot{\theta}_{2y} C_{2x} S_{2y}]^\top. \end{aligned} \quad (13)$$

The outputs of the fuzzy rules are the control gains adjustment $\Delta k_{px}, \Delta k_{py}, \Delta k_{pz}, \Delta k_{dx}, \Delta k_{dy}, \Delta k_{dz}$. Membership function values are assigned to the linguistic variables, using seven fuzzy subsets: negative big (NB), negative medium (NM), negative small (NS), zero (ZE), positive small (PE), positive medium (PM), and positive big (PB). Trimf and Gaussmf type functions are selected as input and output membership functions, the specific form are presented in Fig. 2. The IF-THEN rules for tuning the control gains are expressed generally as follows.

If E_i is MF_j and EC_i is MF_k, THEN k_{pi} is P_{jk} and k_{di} is D_{jk}, where $i = x, y, z$ and $j, k = 1, \dots, 7$, MF_j, MF_k, P_{jk} and D_{jk} represent different membership functions.

TABLE I
FUZZY RULES

$\Delta k_{pi}/\Delta k_{di}$		E_i						
		NB	NM	NS	ZE	PS	PM	PB
EC _i	NB	PB/PS	PB/PS	PM/ZE	PM/ZE	PS/ZE	PS/PB	ZE/PB
	NM	PB/NS	PB/NS	PM/NS	PM/NS	PS/ZE	ZE/NS	ZE/PM
	NS	PM/NB	PM/NB	PM/NM	PS/NS	ZE/ZE	NS/PS	NM/PM
	ZE	PM/NB	PS/NM	PS/NM	ZE/NS	NS/ZE	NM/PS	NM/PM
	PS	PS/NB	PS/NM	ZE/NS	NS/NS	NS/ZE	NM/PS	NM/PS
	PM	ZE/NM	ZE/NS	NS/NS	NM/NS	NM/ZE	NM/PS	NB/PS
	PB	ZE/PS	NS/ZE	NS/ZE	NM/ZE	NB/PB	NB/PB	

The total fuzzy rules are given in Table I. Thus, the adaptive adjustment of the control gains are presented as

$$K_p = \text{diag}([k_{px}, k_{py}, k_{pz}, k_{pl}]) + k_e \text{diag}([\Delta k_{px}, \Delta k_{py}, \Delta k_{pz}, 0])$$

$$K_d = \text{diag}([k_{dx}, k_{dy}, k_{dz}, k_{dl}]) + k_e \text{diag}([\Delta k_{dx}, \Delta k_{dy}, \Delta k_{dz}, 0])$$

where $k_{px}, k_{py}, k_{pz}, k_{pl}, k_{dx}, k_{dy}, k_{dz}, k_{dl}$ are the initial fixed control gains, k_e is a positive parameter.

B. Stability Analysis

Theorem 1: Considering the hook effect, for the aerial transportation system with variable-length cable, the following two points are guaranteed under the proposed control scheme (10) and the update law (11).

- 1) The error system depicted by (5) converges to zero asymptotically, i.e.,

$$\begin{aligned} & \lim_{t \rightarrow \infty} [\mathbf{e}_\alpha^\top, \Theta_1^\top, \Theta_2^\top, \dot{\mathbf{e}}_\alpha^\top, \dot{\Theta}_1^\top, \dot{\Theta}_2^\top]^\top \\ &= [\mathbf{0}_{4 \times 1}^\top, \mathbf{0}_{2 \times 1}^\top, \mathbf{0}_{2 \times 1}^\top, \mathbf{0}_{4 \times 1}^\top, \mathbf{0}_{2 \times 1}^\top, \mathbf{0}_{2 \times 1}^\top]^\top. \end{aligned}$$

- 2) The cable length $l(t)$ satisfies that $0 < l_{\min} < l(t) < l_{\max}$.

Proof: To prove Theorem 1, a scalar function is constructed as follows:

$$\begin{aligned} V &= E + \frac{1}{2} \mathbf{e}_\alpha^\top K_p \mathbf{e}_\alpha + \frac{1}{2} k_s \sec(\varpi_\pi(l - \varpi_l)^2) \rho^2 \\ &+ \frac{1}{2} \sum_{i=x,y,z,l} \tilde{\omega}_i^\top \Upsilon_i^{-1} \tilde{\omega}_i \end{aligned} \quad (14)$$

where $\tilde{\omega}_i = \omega_i - \hat{\omega}_i$, $i = x, y, z, l$ is the estimation error, and one has $\dot{\tilde{\omega}}_i = -\dot{\hat{\omega}}_i$. In the open set $\Phi = \{l : l_{\min} < l < l_{\max}\}$, one has $1 \leq \sec(\varpi_\pi(l - \varpi_l)^2) < +\infty$, which indicates that V is positive definite. When l approaches the boundary of Φ , V will tend to infinity.

Subsequently, substituting (10) and (11) into the time derivative of (14), one can obtain that

$$\begin{aligned} \dot{V} &= \dot{E} + \dot{\mathbf{e}}_\alpha^\top K_p \mathbf{e}_\alpha + k_s \frac{\sin(\varpi_\pi(l - \varpi_l)^2) \varpi_\pi(l - \varpi_l) \dot{l}}{\cos^2(\varpi_\pi(l - \varpi_l)^2)} \rho^2 \\ &+ k_s \frac{\rho(\dot{e}_l - \eta\rho)}{\cos(\varpi_\pi(l - \varpi_l)^2)} - \sum_{i=x,y,z,l} \tilde{\omega}_i^\top \Upsilon_i^{-1} \dot{\tilde{\omega}}_i \\ &= \dot{\mathbf{e}}_\alpha^\top (\mathbf{f} - (M + m_h + m_p) g \mathbf{r}_3 + (m_h + m_p) g \mathbf{r}_4 + K_p \mathbf{e}_\alpha) \end{aligned}$$

$$\begin{aligned} & -\Phi_\alpha) + k_s \frac{\sin(\varpi_\pi(l - \varpi_l)^2) \varpi_\pi(l - \varpi_l) \rho^2}{\cos^2(\varpi_\pi(l - \varpi_l)^2)} \dot{e}_l \\ & + k_s \sec(\varpi_\pi(l - \varpi_l)^2) \rho \dot{e}_l - k_s \eta \sec(\varpi_\pi(l - \varpi_l)^2) \rho^2 \\ & + \sum_{i=x,y,z,l} \tilde{\omega}_i^\top \phi_i \dot{\mathbf{e}}_i - [\dot{\Theta}_1^\top, \dot{\Theta}_2^\top] \Psi [\dot{\Theta}_1^\top, \dot{\Theta}_2^\top]^\top \\ & = -\dot{\mathbf{e}}_\alpha^\top K_d \dot{\mathbf{e}}_\alpha - k_s \eta \sec(\varpi_\pi(l - \varpi_l)^2) \rho^2 + \dot{\mathbf{e}}_\alpha^\top \hat{\Phi}_\alpha \\ & - \dot{\mathbf{e}}_\alpha^\top \Phi_\alpha + \sum_{i=x,y,z,l} \tilde{\omega}_i^\top \phi_i \dot{\mathbf{e}}_i - [\dot{\Theta}_1^\top, \dot{\Theta}_2^\top] \Psi [\dot{\Theta}_1^\top, \dot{\Theta}_2^\top]^\top \\ & = -\dot{\mathbf{e}}_\alpha^\top K_d \dot{\mathbf{e}}_\alpha - k_s \eta \sec(\varpi_\pi(l - \varpi_l)^2) \rho^2 \\ & - [\dot{\Theta}_1^\top, \dot{\Theta}_2^\top] \Psi [\dot{\Theta}_1^\top, \dot{\Theta}_2^\top]^\top. \end{aligned} \quad (15)$$

Since $l(0) \in \Phi$ is satisfied, there must exist sometime T such that when $t \in [0, T]$, $l(t)$ is kept within the corresponding range, i.e., $l(t) \in \Phi$. Thus, when $t \in [0, T]$, one can obtain that $k_s \eta \sec(\varpi_\pi(l - \varpi_l)^2) > 0$. Further, from (14) and (15), it is found that when $t \in [0, T]$, one has $V(t) \geq 0$ and $\dot{V}(t) \leq 0$, which means $V(t) \in L_\infty$. Assume that there exists a $l(t)$ tending to approach the boundary of Φ at time T . Taking the upper bound l_{\max} , for example, i.e., $l(T) = l_{\max}$. Thus, one must first obtain $\lim_{t \rightarrow T^-} l(t) = l_{\max}$, which leads to $\lim_{t \rightarrow T^-} V(t) = +\infty$. It is obviously contrastive with $V(t) \in L_\infty, \forall t \in [0, T]$. By implementing the similar analysis for the lower bound of l , one can conclude that $\dot{V}(t) \leq 0, \forall t \geq 0$ is always valid during the control process, and $l(t)$ is always in Φ , i.e.,

$$0 < l_{\min} < l(t) < l_{\max}. \quad (16)$$

Hence, selecting (14) as the Lyapunov function candidate, based on the aforementioned analysis, the following conclusion can be derived:

$$\begin{aligned} & V \in \mathcal{L}_\infty, e_x, e_y, e_z, e_l, \dot{\theta}_{1x}, \dot{\theta}_{1y}, \dot{\theta}_{2x}, \dot{\theta}_{2y} \in \mathcal{L}_\infty, \rho \in \mathcal{L}_\infty \\ & \dot{x}, \dot{y}, \dot{z}, \dot{l} \Rightarrow \dot{e}_x, \dot{e}_y, \dot{e}_z, \dot{e}_l \in \mathcal{L}_\infty, \tilde{\omega}_\alpha \in \mathcal{L}_\infty \Rightarrow \hat{\omega}_\alpha \in \mathcal{L}_\infty. \end{aligned} \quad (17)$$

Since $l(t)$ is always in Φ , from (8), one can conclude that $f_{lp} \in \mathcal{L}_\infty$. Thus, from (10), it can be derived that $\mathbf{f} \in \mathcal{L}_\infty$. Therefore, combining with the abovementioned analysis, it is not difficult to conclude that the system state variables are all bounded.

Subsequently, the proof of Theorem 1 will be completed with the aid of LaSalle's invariance theorem [30]. Define a set Δ as

$$\Delta = \{(e_q, \dot{e}_q) | \dot{V}(t) = 0\}$$

and let Γ be the largest invariant set in Δ . According to (15), in the largest invariant set Γ , one can draw the following conclusion:

$$\begin{aligned} & \dot{e}_x = \dot{e}_y = \dot{e}_z = \dot{e}_l = 0, \dot{x} = \dot{y} = \dot{z} = \dot{l} = 0 \\ & \dot{\theta}_{1x} = \dot{\theta}_{1y} = \dot{\theta}_{2x} = \dot{\theta}_{2y} = 0, \rho = 0. \end{aligned} \quad (18)$$

Then, taking the time derivative of (18) yields

$$\ddot{x} = \dot{y} = \dot{z} = \ddot{l} = 0, \ddot{\theta}_{1x} = \ddot{\theta}_{1y} = \ddot{\theta}_{2x} = \ddot{\theta}_{2y} = 0. \quad (19)$$

Integrating (18) with respect to time, one has

$$e_x = \beta_x, e_y = \beta_y, e_z = \beta_z, e_l = \beta_l \quad (20)$$

where $\beta_x, \beta_y, \beta_z, \beta_l \in \mathbb{R}$ represent the undetermined constants. Therewith, substituting (18) and (19) into (29)–(32) yields

$$(m_h + m_p)glS_{1x}C_{1y} = 0, m_pgcS_{2x}C_{2y} = 0 \\ (m_h + m_p)glC_{1x}S_{1y} = 0, m_pgcC_{2x}S_{2y} = 0. \quad (21)$$

According to Assumption 2, from (21), one can directly obtain that

$$\theta_{1x} = \theta_{1y} = \theta_{2x} = \theta_{2y} = 0. \quad (22)$$

With the help of (18), substituting (20) into (10) results in

$$\mathbf{f} = -K_p[\beta_x, \beta_y, \beta_z, \beta_l]^\top + (M + m_h + m_p)gr_3 \\ - (m_h + m_p)gr_4. \quad (23)$$

Furthermore, substituting (23) into (25)–(28), and noting (19) and (22), one can obtain

$$-K_p[\beta_x, \beta_y, \beta_z, \beta_l]^\top = \mathbf{0}_{4 \times 1}$$

from which one can conveniently derive that

$$\beta_x = \beta_y = \beta_z = \beta_l = 0 \Rightarrow e_x = e_y = e_z = e_l = 0. \quad (24)$$

In conclusion, one can summarize from (16), (18), (22), and (24) that, Γ only contains the closed-loop equilibrium point. Therefore, by invoking LaSalle's invariance theorem, the proof is completed. ■

IV. SIMULATION AND RESULTS

In this section, two groups of simulation examples are given to reveal the effectiveness and superiority of the proposed fuzzy-based antiswing control algorithm for variable-length cable-suspended aerial transportation system considering the hook effect. The physical parameters of the aerial transportation system are given as follows: $M = 1.5 \text{ kg}$, $m_h = 0.1 \text{ kg}$, $m_p = 0.2 \text{ kg}$, $c = 0.3 \text{ m}$, $g = 9.8 \text{ m/s}^2$. The fixed control gains are set as $k_{px} = 4$, $k_{py} = 4$, $k_{pz} = 6$, $k_{pl} = 4$, $k_{dx} = 5$, $k_{dy} = 5$, $k_{dz} = 7$, $k_{dl} = 2$, $\Upsilon_x = \Upsilon_y = \Upsilon_z = \Upsilon_l = \text{diag}([0.1, 0.1, 0.1])$, $k_s = 0.2$, $k_e = 3$.

A. Basic Performance Test

To evaluate the performance of the proposed control method and the update law when dealing with parameter uncertainties, the following three groups of tests are implemented by setting different unknown resistance coefficients, i.e.,

- 1) $D_\xi = \text{diag}([0.12, 0.12, 0.12])$, $d_l = 0.05$, $d_h = 0.05$, $d_p = 0.08$;
- 2) $D_\xi = \text{diag}([0.50, 0.50, 0.50])$, $d_l = 0.50$, $d_h = 0.10$, $d_p = 0.12$;
- 3) $D_\xi = \text{diag}([1.05, 1.05, 1.05])$, $d_l = 0.50$, $d_h = 0.15$, $d_p = 0.18$.

The initial and the desired states of the multirotor and the cable are set as $\alpha(0) = [3.0, 1.0, 3.0, 5.0]^\top \text{ m}$ and $\alpha_d =$

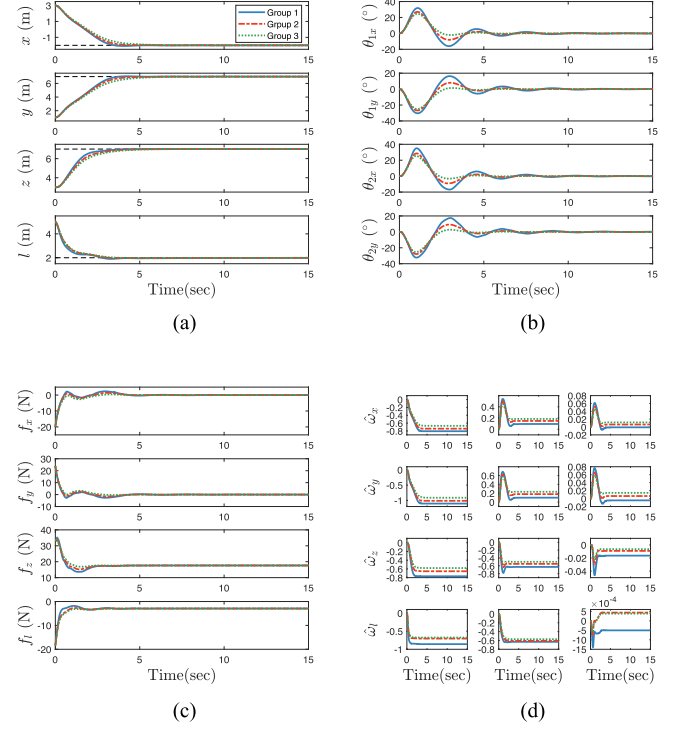


Fig. 3. Results for basic performance test. (Blue solid lines: Results for Group 1. Red dotted lines: Results for Group 2. Green dotted lines: Results for Group 3. Black dotted lines: Desired states.). (a) Multirotor position and cable length. (b) Hook and payload swing angle. (c) Control inputs. (d) Parameter estimates.

$[-2.0, 7.0, 7.0, 2.0]^\top \text{ m}$, respectively. The range of the cable length is set as $(l_{\min}, l_{\max}) = (1.0, 6.0) \text{ m}$. In this test, the domain of the fuzzy rules inputs E_i and EC_i are set as $[-3, 3]$ and $[-8, 8]$, respectively, and the domain of the output Δk_{pi} and Δk_{di} are all set as $[-1, 1]$. The obtained simulation curves are illustrated in Fig. 3, from which it can be observed that under different resistance coefficients, the multirotor and the cable length can track the desired values precisely, and the hook and payload swing angles are quickly suppressed. Besides, the adaptive update law can effectively deal with different resistance coefficients, and the estimations converge eventually.

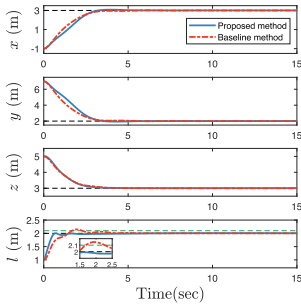
B. Comparison Test

In this section, two sets of comparative tests are carried out. The control gains K_p and K_d of the proposed method consist of two parts, the fixed part control gain is identified to ensure precise positioning of the multirotor and the autotuning part is utilized to dynamically adjust the gains according to the motion of the hook/payload during flight. Thus, to test the performance of the proposed method in hook/payload swing suppression, a baseline control scheme with fixed control gains is selected as the comparison method using the same fixed control gains as those in the proposed method. The specific form of the comparison method is

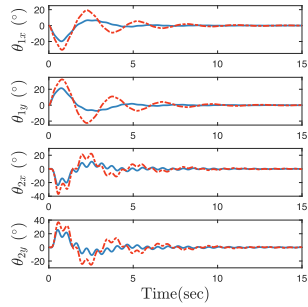
$$\mathbf{f} = -K_{pc}\mathbf{e}_\alpha - K_{dc}\dot{\mathbf{e}}_\alpha + (M + m_h + m_p)gr_3 \\ - (m_h + m_p)gr_4$$

TABLE II
QUANTITATIVE DATA

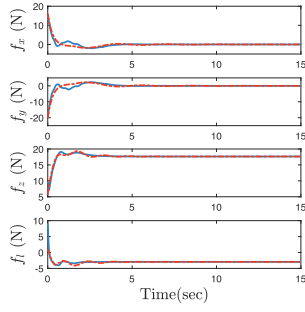
		max				Mean				RMS			
		$\theta_{1x}(\circ)$	$\theta_{1y}(\circ)$	$\theta_{2x}(\circ)$	$\theta_{2y}(\circ)$	$\theta_{1x}(\circ)$	$\theta_{1y}(\circ)$	$\theta_{2x}(\circ)$	$\theta_{2y}(\circ)$	$\theta_{1x}(\circ)$	$\theta_{1y}(\circ)$	$\theta_{2x}(\circ)$	$\theta_{2y}(\circ)$
Test 1	Proposed	19.76	21.34	23.96	25.66	2.07	2.35	2.39	2.70	4.63	5.12	5.04	5.53
	Baseline	30.47	32.37	36.81	36.83	4.35	5.14	4.48	5.24	7.99	9.17	8.61	9.68
Test 2	Proposed	16.98	18.99	18.85	20.65	2.24	2.63	2.70	3.16	4.27	4.87	4.61	5.26
	Proposed	23.72	26.69	25.31	28.12	3.71	4.48	4.04	4.85	6.45	7.62	6.89	8.08



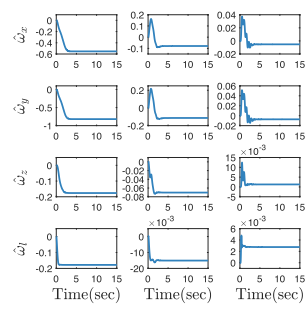
(a)



(b)



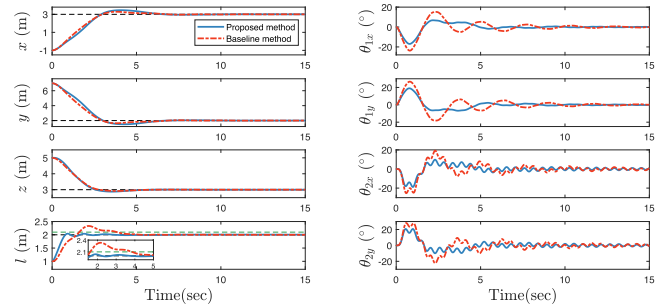
(c)



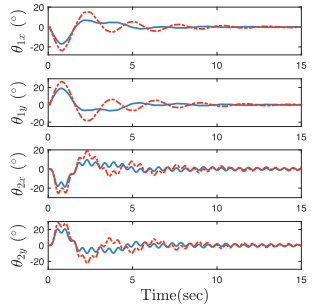
(d)

Fig. 4. Results for Comparison Test 1. (Blue solid lines: Results by the proposed method. Red dotted lines: Results by the baseline method. Black dotted lines: Desired states.). (a) Multirotor position and cable length. (b) Hook and payload swing angle. (c) Control inputs. (d) Parameter estimates.

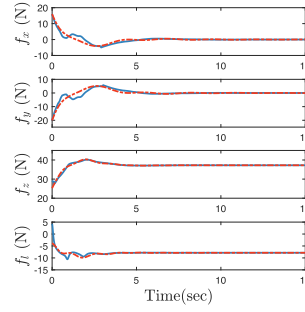
where $K_{pc} = \text{diag}([4, 4, 6, 4])$ and $K_{dc} = \text{diag}([5, 5, 7, 2])$ are set the same as the fixed part control gains of the proposed method. The initial and desired positions of the multicopter are $\xi(0) = [-1.0, 7.0, 5.0]^\top$ m and $\xi_d = [3.0, 2.0, 3.0]^\top$ m. The initial and desired cable lengths are $l(0) = 2.0$ m and $l_d = 1.0$ m. The cable length constraint is set as $(l_{\min}, l_{\max}) = (0.9, 2.1)$ m. The resistance coefficients is set the same as that of the first group of basic performance test. The domain of the fuzzy rules inputs E_i and EC_i are set as $[-1.5, 1.5]$ and $[-5, 5]$, respectively, and the domain of the output Δk_{pi} and Δk_{di} are all set as $[-1, 1]$. The simulation results are recorded by Fig. 4 and the explicit quantified data on absolute maximum, absolute mean, and root mean square (RMS) values of hook/payload swing angles are collected by Table II. It can be observed that both control schemes can drive the multicopter to the desired position with similar transportation efficiency. Meanwhile, the cable length can be adjusted to the desired value accurately. However, due to the constraint imposed on the cable length, the maximum



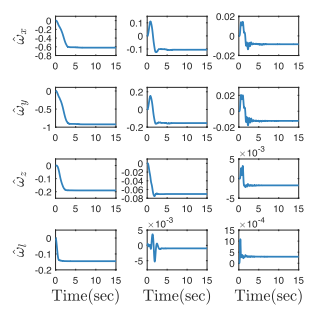
(a)



(b)



(c)



(d)

Fig. 5. Results for Comparison Test 2. (Blue solid lines: Results by the proposed method. Red dotted lines: Results by the baseline method. Black dotted lines: Desired states.). (a) Multirotor position and cable length. (b) Hook and payload swing angle. (c) Control inputs. (d) Parameter estimates.

length under the proposed method is consistently guaranteed to be within 2.1 m, while cable length of the comparison method exceeds the limit. From Fig. 4(b) and Table II, one finds that the maximum hook/payload swing angles by the proposed method is much smaller than that of the baseline control method. The maximum value of all swing angles of the comparison method is almost 1.5 times that of the proposed method, which proves the excellent performance of the employed fuzzy rules in restraining hook/payload swing angles.

To further verify the robustness of the proposed method to the system parameters, we adjust the mass of the multicopter, hook, and payload, as well as the distance between the hook and payload, specifically as, $M = 3.0$ kg, $m_h = 0.3$ kg, $m_p = 0.5$ kg, $c = 0.2$ m. The resulted curves are given in Fig. 5, from which one can find that both methods can drive the system to the desired state in terms of multicopter positioning and cable length adjustment. Moreover, combining with Table II, one can well perceive that even under different system parameters, the proposed method presents an excellent performance

in hook/payload anti-swing compared to the baseline controller, the absolute maximum, absolute mean, and RMS values of these angles in the proposed method are all smaller than those in the baseline method.

V. CONCLUSION

This article establishes the dynamic model of the variable-length cable-suspended aerial transportation system considering the hook effect, and develops a fuzzy-based antiswing control law to achieve multirotor positioning, cable length adjusting and hook/payload swing elimination. To avoid the collision between the hook and the multirotor during transportation, a cable length constraint term is constructed to ensure that the cable length always changes within the allowable range. The stability of the closed-loop system is guaranteed by Lyapunov techniques and LaSalle's invariance theorem. Two groups of simulation tests are conducted to verify the effectiveness of the proposed method in dealing with different resistance coefficients and restraining hook/payload swing during transportation. In the ensuing research, the smooth payload release control will be further studied under the consideration of the hook effect.

APPENDIX A

The dynamic model (3) can be expanded as

$$\begin{aligned} & (M + m_h + m_p) \ddot{x} + (m_h + m_p) \left(\ddot{l} C_{1y} S_{1x} + 2\dot{l} \dot{\theta}_{1x} C_{1x} C_{1y} - 2\dot{l} \dot{\theta}_{1y} S_{1x} S_{1y} \right) + (m_h + m_p) l \left(\ddot{\theta}_{1x} C_{1x} C_{1y} - \ddot{\theta}_{1y} S_{1x} S_{1y} - \dot{\theta}_{1x}^2 S_{1x} C_{1y} - \dot{\theta}_{1y}^2 C_{1y} S_{1x} - 2\dot{\theta}_{1x} \dot{\theta}_{1y} C_{1x} S_{1y} \right) + m_p c \cdot \\ & \left(\ddot{\theta}_{2x} C_{2x} C_{2y} - \ddot{\theta}_{2y} S_{2x} S_{2y} - \dot{\theta}_{2x}^2 S_{2x} C_{2y} - \dot{\theta}_{2y}^2 C_{2y} S_{2x} - 2\dot{\theta}_{2x} \dot{\theta}_{2y} C_{2x} S_{2y} \right) = f_x + f_{rx} \end{aligned} \quad (25)$$

$$\begin{aligned} & (M + m_h + m_p) \ddot{y} + (m_h + m_p) \left(\ddot{l} S_{1y} + 2\dot{l} \dot{\theta}_{1y} C_{1y} \right) + (m_h + m_p) l \left(\ddot{\theta}_{1y} C_{1y} - \dot{\theta}_{1y}^2 S_{1y} \right) + m_p c \left(\ddot{\theta}_{2y} C_{2y} - \dot{\theta}_{2y}^2 S_{2y} \right) = f_y + f_{ry} \end{aligned} \quad (26)$$

$$\begin{aligned} & (M + m_h + m_p) \ddot{z} - (m_h + m_p) \left(\ddot{l} C_{1x} C_{1y} - 2\dot{l} \dot{\theta}_{1x} S_{1x} C_{1y} - 2\dot{l} \dot{\theta}_{1y} C_{1x} S_{1y} \right) + (m_h + m_p) l \left(\ddot{\theta}_{1x} S_{1x} C_{1y} + \ddot{\theta}_{1y} C_{1x} S_{1y} + \dot{\theta}_{1x}^2 C_{1x} C_{1y} + \dot{\theta}_{1y}^2 C_{1x} C_{1y} - 2\dot{\theta}_{1x} \dot{\theta}_{1y} S_{1x} S_{1y} \right) + m_p c \cdot \\ & \left(\ddot{\theta}_{2x} S_{2x} C_{2y} + \ddot{\theta}_{2y} C_{2x} S_{2y} + \dot{\theta}_{2x}^2 C_{2x} C_{2y} + \dot{\theta}_{2y}^2 C_{2x} C_{2y} - 2\dot{\theta}_{2x} \dot{\theta}_{2y} S_{2x} S_{2y} \right) + (M + m_h + m_p) g = f_z + f_{rz} \end{aligned} \quad (27)$$

$$\begin{aligned} & (m_h + m_p) \left(\ddot{x} S_{1x} C_{1y} + \ddot{y} S_{1y} - \ddot{z} C_{1x} C_{1y} + \ddot{l} - l \dot{\theta}_{1x}^2 C_{1y}^2 - l \dot{\theta}_{1y}^2 - g C_{1x} C_{1y} \right) + m_p c \left(C_{1y} C_{2y} S_{1x-2x} \ddot{\theta}_{2x} + \ddot{\theta}_{2y} S_{1y} C_{2y} \right) \end{aligned}$$

$$\begin{aligned} & -C_{1y} S_{2y} C_{1x-2x} \ddot{\theta}_{2y} - \dot{\theta}_{2x}^2 C_{1y} C_{2y} C_{1x-2x} - \dot{\theta}_{2y}^2 S_{1y} S_{2y} \\ & - \dot{\theta}_{2y}^2 C_{1y} C_{2y} C_{1x-2x} - 2\dot{\theta}_{2x} \dot{\theta}_{2y} C_{1y} S_{2y} S_{1x-2x} \Big) = f_l + f_{rl} \end{aligned} \quad (28)$$

$$\begin{aligned} & (m_h + m_p) l C_{1y} \left(\ddot{x} C_{1x} + \ddot{z} S_{1x} + l \dot{\theta}_{1x} C_{1y} + 2l \dot{\theta}_{1x} C_{1y} \right. \\ & \left. - 2l \dot{\theta}_{1x} \dot{\theta}_{1y} S_{1y} + g S_{1x} \right) + m_p l c C_{1y} \left(C_{2y} C_{1x-2x} \ddot{\theta}_{2x} \right. \\ & \left. + S_{2y} S_{1x-2x} \ddot{\theta}_{2y} + \dot{\theta}_{2x}^2 C_{2y} S_{1x-2x} + \dot{\theta}_{2y}^2 C_{2y} S_{1x-2x} \right. \\ & \left. - 2\dot{\theta}_{2x} \dot{\theta}_{2y} S_{2y} C_{1x-2x} \right) = f_{r\theta_{1x}} \end{aligned} \quad (29)$$

$$\begin{aligned} & (m_h + m_p) l \left(-\ddot{x} S_{1x} S_{1y} + \ddot{y} C_{1y} + \ddot{z} C_{1x} S_{1y} + l \ddot{\theta}_{1y} + 2l \dot{\theta}_{1y} \right. \\ & \left. + l \dot{\theta}_{1x}^2 C_{1y} S_{1y} + g C_{1x} S_{1y} \right) + m_p l c \left(-S_{1y} C_{2y} S_{1x-2x} \ddot{\theta}_{2x} \right. \\ & \left. + S_{1y} S_{2y} C_{1x-2x} \ddot{\theta}_{2y} + \dot{\theta}_{2y} C_{1y} C_{2y} + \dot{\theta}_{2x}^2 S_{1y} C_{2y} C_{1x-2x} \right. \\ & \left. + \dot{\theta}_{2y}^2 S_{1y} C_{2y} C_{1x-2x} + 2\dot{\theta}_{2x} \dot{\theta}_{2y} S_{1y} S_{2y} S_{1x-2x} - \dot{\theta}_{2y}^2 C_{1y} S_{2y} \right) \\ & = f_{r\theta_{1y}} \end{aligned} \quad (30)$$

$$\begin{aligned} & m_p c C_{2y} \left(\ddot{x} C_{2x} + \ddot{z} S_{2x} + l \ddot{C}_{1y} S_{1x-2x} + l \ddot{\theta}_{1x} C_{1y} C_{1x-2x} \right. \\ & \left. - l \ddot{\theta}_{1y} S_{1y} S_{1x-2x} + c \ddot{\theta}_{2x} C_{2y} - 2c \dot{\theta}_{2x} \dot{\theta}_{2y} S_{2y} - l \dot{\theta}_{1x}^2 C_{1y} S_{1x-2x} \right. \\ & \left. - l \dot{\theta}_{1y}^2 C_{1y} S_{1x-2x} - 2l \dot{\theta}_{1x} \dot{\theta}_{1y} S_{1y} C_{1x-2x} + 2l \dot{\theta}_{1x} C_{1y} C_{1x-2x} \right. \\ & \left. - 2l \dot{\theta}_{1y} S_{1y} S_{1x-2x} + g S_{2x} \right) = f_{r\theta_{2x}} \end{aligned} \quad (31)$$

$$\begin{aligned} & m_p c \left(-\ddot{x} S_{2x} S_{2y} + \ddot{y} C_{2y} + \ddot{z} C_{2x} S_{2y} + l \ddot{S}_{1y} C_{2y} + l \ddot{\theta}_{1y} C_{1y} C_{2y} \right. \\ & \left. - l \ddot{C}_{1y} S_{2y} C_{1x-2x} + l \ddot{\theta}_{1x} C_{1y} S_{2y} S_{1x-2x} + l \ddot{\theta}_{1y} S_{1y} S_{2y} C_{1x-2x} \right. \\ & \left. + l \dot{\theta}_{1x}^2 C_{1y} S_{2y} C_{1x-2x} + l \dot{\theta}_{1y}^2 C_{1y} S_{2y} C_{1x-2x} + c \dot{\theta}_{2x}^2 C_{2y} S_{2y} \right. \\ & \left. + c \ddot{\theta}_{2y} + 2l \dot{\theta}_{1x} C_{1y} S_{2y} S_{1x-2x} + 2l \dot{\theta}_{1y} C_{1y} C_{2y} - l \dot{\theta}_{1y}^2 S_{1y} C_{2y} \right. \\ & \left. + 2l \dot{\theta}_{1y} S_{1y} S_{2y} C_{1x-2x} - 2l \dot{\theta}_{1x} \dot{\theta}_{1y} S_{1y} S_{2y} S_{1x-2x} + g C_{2x} S_{2y} \right) \\ & = f_{r\theta_{2y}} \end{aligned} \quad (32)$$

where $f_{rx}, f_{ry}, f_{rz}, f_{rl}, f_{r\theta_{1x}}, f_{r\theta_{1y}}, f_{r\theta_{2x}}, f_{r\theta_{2y}} \in \mathbb{R}$ denote the resistance forces, whose specific form are

$$\begin{aligned} f_{rx} &= -d_x \dot{x} - d_h \dot{x} - d_p \dot{x} - d_h \dot{l} C_{1y} S_{1x} - d_h \dot{\theta}_{1x} l C_{1x} C_{1y} \\ &+ d_h \dot{\theta}_{1y} l S_{1x} S_{1y} - d_p \dot{l} C_{1y} S_{1x} - d_p \dot{\theta}_{1x} l C_{1x} C_{1y} \\ &+ d_p \dot{\theta}_{1y} l S_{1x} S_{1y} - c d_p \dot{\theta}_{2x} C_{2x} C_{2y} + c d_p \dot{\theta}_{2y} S_{2x} S_{2y} \\ f_{ry} &= -d_y \dot{y} - d_h \dot{y} - d_p \dot{y} - d_h \dot{l} S_{1y} - d_h \dot{\theta}_{1y} l C_{1y} - d_p \dot{l} S_{1y} \\ &- d_p \dot{\theta}_{1y} l C_{1y} - c d_p \dot{\theta}_{2y} C_{2y} \\ f_{rz} &= -d_z \dot{z} - d_h \dot{z} - d_p \dot{z} + d_h \dot{l} C_{1x} C_{1y} - d_h \dot{\theta}_{1x} l C_{1y} S_{1x} \\ &- d_h \dot{\theta}_{1y} l C_{1x} S_{1y} + d_p \dot{l} C_{1x} C_{1y} - d_p \dot{\theta}_{1x} l C_{1y} S_{1x} \\ &- d_p \dot{\theta}_{1y} l C_{1x} S_{1y} - c d_p \dot{\theta}_{2x} C_{2x} S_{2y} - c d_p \dot{\theta}_{2y} C_{2x} S_{2y} \end{aligned}$$

$$\begin{aligned}
f_{rl} = & -d_l \dot{l} - d_h \dot{l} - d_p \dot{l} - d_h \dot{x} C_{1y} S_{1x} - d_h \dot{y} S_{1y} + d_h \dot{z} C_{1x} C_{1y} \\
& - d_p \dot{x} C_{1y} S_{1x} - d_p \dot{y} S_{1y} + d_p \dot{z} C_{1x} C_{1y} - c d_p \dot{\theta}_{2y} C_{2y} S_{1y} \\
& - c d_p \dot{\theta}_{2x} C_{1y} C_{2y} S_{1x-2x} + c d_p \dot{\theta}_{2y} C_{1y} S_{2y} C_{1x-2x} \\
f_{r\theta_{1x}} = & -l C_{1y} \left(d_h \dot{x} C_{1x} + d_h \dot{z} S_{1x} + d_h \dot{\theta}_{1x} l C_{1y} + d_p \dot{x} C_{1x} + d_p \dot{z} S_{1x} \right. \\
& \left. + d_p \dot{\theta}_{1x} l C_{1y} + c d_p \dot{\theta}_{2x} C_{2y} C_{1x-2x} + c d_p \dot{\theta}_{2y} S_{1x-2x} S_{2y} \right) \\
f_{r\theta_{1y}} = & d_h \dot{x} l S_{1x} S_{1y} - d_h \dot{y} l C_{1y} - d_h \dot{z} l C_{1x} S_{1y} - d_h \dot{\theta}_{1y} l^2 \\
& + d_p \dot{x} l S_{1x} S_{1y} - d_p \dot{y} l C_{1y} - d_p \dot{z} l C_{1x} S_{1y} - d_p \dot{\theta}_{1y} l^2 \\
& + c d_p \dot{\theta}_{2x} l C_{2y} S_{1y} S_{1x-2x} - c d_p \dot{\theta}_{2y} l S_{1y} S_{2y} C_{1x-2x} \\
& - c d_p \dot{\theta}_{2y} l C_{1y} C_{2y} \\
f_{r\theta_{2x}} = & -c d_p C_{2y} \left(\dot{x} C_{2x} + \dot{z} S_{2x} + c \dot{\theta}_{2x} C_{2y} + l C_{1y} S_{1x-2x} \right. \\
& \left. + \dot{\theta}_{1x} l C_{1y} C_{1x-2x} - \dot{\theta}_{1y} l S_{1y} S_{1x-2x} \right) \\
f_{r\theta_{2y}} = & -c d_p \left(-\dot{x} S_{2x} S_{2y} + \dot{y} C_{2y} + l C_{2y} S_{1y} + \dot{z} C_{2x} S_{2y} \right. \\
& \left. + c \dot{\theta}_{2y} + \dot{\theta}_{1y} l C_{1y} C_{2y} + \dot{\theta}_{1x} l C_{1y} S_{2y} S_{1x-2x} \right. \\
& \left. - l C_{1y} S_{2y} C_{1x-2x} + \dot{\theta}_{1y} l S_{1y} S_{2y} C_{1x-2x} \right)
\end{aligned}$$

where $d_x, d_y, d_z, d_l, d_h, d_p \in \mathbb{R}_+$ stand for the corresponding damping coefficients.

APPENDIX B

The damping coefficient vectors $\omega_x, \omega_y, \omega_z, \omega_l \in \mathbb{R}^3$ and the composite velocity signal vectors $\phi_x, \phi_y, \phi_z, \phi_l \in \mathbb{R}^3$ are listed as

$$\begin{aligned}
\omega_i = & [d_i + d_h + d_p, d_h + d_p, d_p]^\top, i = x, y, z, l \\
\phi_x = & \left[\dot{x}, \dot{l} S_{1x} C_{1y} + 2l \left(\dot{\theta}_{1x} C_{1x} C_{1y} - \dot{\theta}_{1y} S_{1x} S_{1y} \right), \right. \\
& \left. 2c \left(\dot{\theta}_{2x} C_{2x} C_{2y} - \dot{\theta}_{2y} S_{2x} S_{2y} \right) \right]^\top \\
\phi_y = & \left[\dot{y}, \dot{l} S_{1y} + 2l \dot{\theta}_{1y} C_{1y}, 2c \dot{\theta}_{2y} C_{2y} \right]^\top \\
\phi_z = & \left[\dot{z}, -\dot{l} C_{1x} C_{1y} + 2l \left(\dot{\theta}_{1x} C_{1y} S_{1x} + \dot{\theta}_{1y} C_{1x} S_{1y} \right), \right. \\
& \left. 2c \left(\dot{\theta}_{2x} C_{2y} S_{2x} + \dot{\theta}_{2y} C_{2x} S_{2y} \right) \right]^\top \\
\phi_l = & \left[\dot{l}, S_{1x} C_{1y} \dot{x} + \dot{S}_{1y} \dot{y} - C_{1x} C_{1y} \dot{z}, 2c \left(\dot{\theta}_{2y} C_{1y} S_{2y} C_{1x-2x} \right. \right. \\
& \left. \left. - \dot{\theta}_{2y} C_{2y} S_{1y} - \dot{\theta}_{2x} C_{1y} C_{2y} S_{1x-2x} \right) \right]^\top.
\end{aligned}$$

APPENDIX C

The detailed expression of Ψ is given as

$$\Psi = \begin{bmatrix} \psi_{11} & \psi_{12} & \psi_{13} & \psi_{14} \\ \psi_{21} & \psi_{22} & \psi_{23} & \psi_{24} \\ \psi_{31} & \psi_{32} & \psi_{33} & \psi_{34} \\ \psi_{41} & \psi_{42} & \psi_{43} & \psi_{44} \end{bmatrix}$$

where $\psi_{11} = d_h l^2 C_{1y}^2 + d_p l^2 C_{1y}^2, \psi_{22} = d_h l^2 + d_p l^2, \psi_{33} = c^2 d_p C_{2y}^2, \psi_{44} = c^2 d_p, \psi_{13} = \psi_{31} = c d_p l C_{1y} C_{2y} C_{1x-2x}, \psi_{14} = \psi_{41} = c d_p l C_{1y} S_{2y} S_{1x-2x}, \psi_{23} = \psi_{32} = -c d_p l C_{2y} S_{1y} S_{1x-2x}, \psi_{24} = \psi_{42} = c d_p l C_{1y} C_{2y} + c d_p l S_{1y} S_{2y} C_{1x-2x}, \psi_{12} = \psi_{21} = \psi_{34} = \psi_{43} = 0$.

Subsequently, Ψ will be proved to be a positive definite matrix. As presented in (7), define $\Psi_\Theta = [\dot{\Theta}_1^\top, \dot{\Theta}_2^\top] \Psi [\dot{\Theta}_1^\top, \dot{\Theta}_2^\top]^\top$, which can be expanded as

$$\begin{aligned}
\Psi_\Theta = & d_h l^2 C_{1y}^2 \dot{\theta}_{1x}^2 + d_h l^2 \dot{\theta}_{1y}^2 + d_p \left(l \dot{\theta}_{1x} C_{1x} C_{1y} - l \dot{\theta}_{1y} S_{1x} S_{1y} \right. \\
& \left. + c \dot{\theta}_{2x} C_{2x} C_{2y} - c \dot{\theta}_{2y} S_{2x} S_{2y} \right)^2 + d_p \left(l \dot{\theta}_{1x} S_{1x} C_{1y} \right. \\
& \left. + l \dot{\theta}_{1y} C_{1x} S_{1y} + c \dot{\theta}_{2x} S_{2x} C_{2y} + c \dot{\theta}_{2y} C_{2x} S_{2y} \right)^2 \\
& + d_p \left(l \dot{\theta}_{1y} C_{1y} + c \dot{\theta}_{2y} C_{2y} \right)^2.
\end{aligned}$$

Therefore, according to Assumption 2, one can know that $\dot{E}_\Theta \geq 0$, if and only if $[\dot{\Theta}_1^\top, \dot{\Theta}_2^\top] = \mathbf{0}_{4 \times 1}, \dot{E}_\Theta = 0$, which indicates that Ψ is a positive definite matrix.

REFERENCES

- [1] I. Lopez-Sanchez and J. Moreno-Valenzuela, "PiD control of quadrotor UAVs: A survey," *Annu. Rev. Control*, vol. 56, 2023, Art. no. 100900.
- [2] L. Kong, Z. Liu, Z. Zhao, and H.-K. Lam, "Observer-based fuzzy tracking control for an unmanned aerial vehicle with communication constraints," *IEEE Trans. Fuzzy Syst.*, vol. 32, no. 6, pp. 3368–3380, Jun. 2024.
- [3] Z. Lv, Q. Zhao, X.-M. Sun, and Y. Wu, "Finite-time control design for a coaxial tilt-rotor UAV," *IEEE Trans. Ind. Electron.*, vol. 71, no. 12, pp. 16132–16142, Dec. 2024.
- [4] Y. Liu, F. Zhang, P. Huang, and Y. Lu, "Configuration optimization and distributed formation control for tethered multirotor UAS," *IEEE/ASME Trans. Mechatron.*, vol. 28, no. 6, pp. 3434–3445, Dec. 2023.
- [5] Z. Yu et al., "Enhanced recurrent fuzzy neural fault-tolerant synchronization tracking control of multiple unmanned airships via fractional calculus and fixed-time prescribed performance function," *IEEE Trans. Fuzzy Syst.*, vol. 30, no. 10, pp. 4515–4529, Oct. 2022.
- [6] Y. Wu, M. Chen, H. Li, and M. Chadli, "Event-triggered-based adaptive NN cooperative control of six-rotor UAVs with finite-time prescribed performance," *IEEE Trans. Autom. Sci. Eng.*, vol. 21, no. 2, pp. 1867–1877, Apr. 2024.
- [7] K. Sreenath, T. Lee, and V. Kumar, "Geometric control and differential flatness of a quadrotor UAV with a cable-suspended load," in *Proc. 52nd IEEE Conf. Decis. Control*, Firenze, Italy, 2013, pp. 2269–2274.
- [8] L. Qian and H. H. Liu, "Path-following control of a quadrotor UAV with a cable-suspended payload under wind disturbances," *IEEE Trans. Ind. Electron.*, vol. 67, no. 3, pp. 2021–2029, Mar. 2020.
- [9] B. Xian and S. Yang, "Robust tracking control of a quadrotor unmanned aerial vehicle-suspended payload system," *IEEE/ASME Trans. Mechatron.*, vol. 26, no. 5, pp. 2653–2663, Oct. 2021.
- [10] J. Zeng, P. Kotaru, M. W. Mueller, and K. Sreenath, "Differential flatness based path planning with direct collocation on hybrid modes for a quadrotor with a cable-suspended payload," *IEEE Robot. Autom. Lett.*, vol. 5, no. 2, pp. 3074–3081, Apr. 2020.
- [11] Y. Ren, Z. Zhao, C. K. Ahn, and H.-X. Li, "Adaptive fuzzy control for an uncertain axially moving slung-load cable system of a hovering helicopter with actuator fault," *IEEE Trans. Fuzzy Syst.*, vol. 30, no. 11, pp. 4915–4925, Nov. 2022.
- [12] G. Yu, D. Cabecinhas, R. Cunha, and C. Silvestre, "Aggressive maneuvers for a quadrotor-slung-load system through fast trajectory generation and tracking," *Auton. Robots*, vol. 46, no. 4, pp. 499–513, 2022.
- [13] X. Liang, Y. Fang, N. Sun, and H. Lin, "Dynamics analysis and time-optimal motion planning for unmanned quadrotor transportation systems," *Mechatronics*, vol. 50, pp. 16–29, 2018.
- [14] F. A. Goodarzi, "Autonomous aerial payload delivery with quadrotor using varying length cable," in *Proc. Int. Conf. Adv. Mechatronic Syst.*, 2016, pp. 394–399.

- [15] J. Zeng, P. Kotaru, and K. Sreenath, "Geometric control and differential flatness of a quadrotor UAV with load suspended from a pulley," in *Proc. Amer. Control Conf.*, 2019, pp. 2420–2427.
- [16] X. Liang, H. Yu, Z. Zhang, H. Liu, Y. Fang, and J. Han, "Unmanned aerial transportation system with flexible connection between the quadrotor and the payload: Modeling, controller design, and experimental validation," *IEEE Trans. Ind. Electron.*, vol. 70, no. 2, pp. 1870–1882, Feb. 2023.
- [17] J. Huang, H. Tao, Y. Wang, and J.-Q. Sun, "Suppressing UAV payload swing with time-varying cable length through nonlinear coupling," *Mech. Syst. Signal Process.*, vol. 185, 2023, Art. no. 109790.
- [18] H. Yu, X. Liang, J. Han, and Y. Fang, "Adaptive trajectory tracking control for the quadrotor aerial transportation system landing a payload onto the mobile platform," *IEEE Trans. Ind. Inform.*, vol. 20, no. 1, pp. 23–37, Jan. 2024.
- [19] H. Yu, Z. Zhang, T. Pei, J. Han, Y. Fang, and X. Liang, "Visual servoing-based anti-swing control of cable-suspended aerial transportation systems with variable-length cable," *IEEE Trans. Autom. Sci. Eng.*, to be published, doi: [10.1109/TASE.2024.3434637](https://doi.org/10.1109/TASE.2024.3434637).
- [20] S. Li, T. T. Duong, and D. Zanotto, "In-flight cable length control for improved quadrotor-based suspended load transportation," *IEEE Robot. Autom. Lett.*, vol. 9, no. 1, pp. 667–674, Jan. 2024.
- [21] J. Estevez, J. M. Lopez-Gude, G. Garate, and M. Graña, "A hybrid control approach for the swing free transportation of a double pendulum with a quadrotor," *Appl. Sci.*, vol. 11, no. 12, 2021, Art. no. 5487.
- [22] J. Qi, Y. Ping, M. Wang, and C. Wu, "Online trajectory planning method for double-pendulum quadrotor transportation systems," *Electronics*, vol. 11, no. 1, 2021, Art. no. 50.
- [23] X. Liang, P. Zhang, Y. Fang, H. Lin, and W. He, "Nonlinear control for aerial transportation systems with double-pendulum swing effects," *IEEE Trans. Ind. Electron.*, vol. 68, no. 7, pp. 6020–6030, Jul. 2021.
- [24] K. Cai, H. Yu, W. He, X. Liang, J. Han, and Y. Fang, "An enhanced-coupling control method for aerial transportation systems with double-pendulum swing effects," *IEEE/ASME Trans. Mechatron.*, vol. 29, no. 3, pp. 2302–2315, Jun. 2024.
- [25] G. Yu, W. Xie, D. Cabecinhas, R. Cunha, and C. Silvestre, "Adaptive control with unknown mass estimation for a quadrotor-slung-load system," *ISA Trans.*, vol. 133, pp. 412–423, 2023.
- [26] H. Li, H. Wang, C. Feng, F. Gao, B. Zhou, and S. Shen, "Autotrans: A complete planning and control framework for autonomous UAV payload transportation," *IEEE Robot. Autom. Lett.*, vol. 8, no. 10, pp. 6859–6866, Oct. 2023.
- [27] Y. Zhu, Z. Zheng, J. Shao, H. Huang, and W. X. Zheng, "Modeling, robust control design, and experimental verification for quadrotor carrying cable-suspended payload," *IEEE Trans. Autom. Sci. Eng.*, to be published, doi: [10.1109/TASE.2024.3437747](https://doi.org/10.1109/TASE.2024.3437747).
- [28] R. Miranda-Carolado and L. T. Aguilar, "A family of anti-swing motion controllers for 2D-crane with load hoisting/lowering," *Mech. Syst. Signal Process.*, vol. 133, 2019, Art. no. 106253.
- [29] G. Li, J. Huang, and S. Gnezdilov, "Dynamics and control of dual-quadrotors slung a slender beam with attitude-pendulum coupling effects," *J. Vib. Control*, vol. 30, no. 9/10, pp. 1995–2005, 2024.
- [30] H. K. Khalil, *Nonlinear Systems*. Upper Saddle River, NJ, USA: Prentice-Hall, 2002.



Hai Yu (Student Member, IEEE) received the B.S. degree in automation from Jilin University, Changchun, China, in 2020. He is currently working toward the Ph.D. degree in control science and engineering with the Institute of Robotics and Automatic Information System, Nankai University, Tianjin, China.

His research interests include nonlinear control of autonomous aerial vehicles.



Yi Chai received the B.S. degree in automation and the M.S. degree in control science and engineering from Harbin Engineering University, Harbin, China, in 2015 and 2018, respectively, and the Ph.D. degree in control science and engineering from Nankai University, Tianjin, China, in 2022.

He is currently a Postdoctoral Fellow with the Institute of Robotics and Automatic Information System, Nankai University. His research interests include motion planning and nonlinear control for collaborative aerial transportation systems.



Zhipiao Yang received the B.S. degree in automation in 2019 from Nankai University, Tianjin, China, where he is currently working toward the Ph.D. degree in control science and engineering with the Institute of Robotics and Automatic Information System, Nankai University, Tianjin, China.

His research interests include motion planning and nonlinear control of autonomous aerial vehicles.



Jiandia Han (Member, IEEE) received the Ph.D. degree in mechatronic engineering from the Harbin Institute of Technology, Harbin, China, in 1998.

From 1998 to 2003, he was a Visiting Scientist with the City University of Hong Kong, Hong Kong, Michigan State University, East Lansing, MI, USA, and Cornell University, Ithaca, NY, USA. He is currently a Professor with the Institute of Robotics and Automatic Information Systems, Nankai University, Tianjin, China. His research interests include nonlinear estimation and control, robotics, and mechatronics systems.



Yongchun Fang (Senior Member, IEEE) received the B.S. and M.S. degrees in control theory and applications from Zhejiang University, Hangzhou, China, in 1996 and 1999, respectively, and the Ph.D. degree in electrical engineering from Clemson University, Clemson, SC, USA, in 2002.

From 2002 to 2003, he was a Postdoctoral Fellow with the Sibley School of Mechanical and Aerospace Engineering, Cornell University, Ithaca, NY, USA. He is currently a Professor with the Institute of Robotics and Automatic Information Systems, Nankai University, Tianjin, China. His research interests include nonlinear control, visual servoing, control of underactuated systems, and atomic force microscopy (AFM)-based nanosystems.

Dr. Fang was the recipient of the National Science Fund for Distinguished Young Scholars of China. He was an Associate Editor for the *ASME Journal of Dynamic Systems, Measurement, and Control*.



Xiaoliang Liang (Senior Member, IEEE) received the B.S. degree in intelligence science and technology from the Hebei University of Technology, Tianjin, China, in 2013 and the Ph.D. degree in control theory and control engineering from Nankai University, Tianjin, China, in 2018.

He is currently an Associate Professor with the Institute of Robotics and Automatic Information System, Nankai University. His research interests include motion planning and nonlinear control of autonomous aerial vehicles systems.